SEDIMENT TRANSPORT ASSESSMENT IN SUSPENSION FLOW BASED ON COHERENT STRUCTURES CHARACTERISTICS

D. Hurther

Laboratoire de Recherches Hydrauliques,

Ecole Polytechnique Fédérale de Lausanne, CH-1015 Lausanne, Switzerland.

Phone: +41 21 693 2400; Fax: + 41 21 693 6767; E-mail : david.hurther@epfl.ch

Abstract: The sediment entrainment ability of coherent flow structures is investigated by comparing higher order statistical properties of shear stress and of turbulent mass fluxes in suspension, open-channel flow under capacity charge conditions. The quadrant repartitions of these quantities as a function of the corresponding threshold levels are estimated using a higher order cumulant discarded probability density distribution of the time fluctuating velocity and concentration fields. Good agreement between the third order model and the experimental results is found for all investigated quantities in the wall and intermediate flow regions. The quadrant distributions of the relative horizontal and vertical mass fluxes are dominated by the same two quadrants as the shear stress. The suspended sediment transport capacity of coherent structures is directly quantified from the estimation of the conditionally sampled terms of the sediment diffusion equation. Coherent structures of a burst cycle are found to be important contributors in the mass transport mechanism under highly turbulent flow conditions in open-channel flows.
Direct estimation of the time scales of coherent structures permitted to correct a novel formulation of the near bed equilibrium concentration proposed recently by Cao (1999).

Keywords: sediment transport, conditional statistics, conditional sampling, coherent structures, suspension flow, ultrasonic sonar

1   INTRODUCTION

Several studies have tried to determine the link between coherent flow structures and sediment transport in different turbulent flows. Sediments are found to respond to different forces in suspension transport and in bed-load transport. Bed-load transport

may arise from pressure fluctuations at the bed while shear stress fluctuations drive the sediment movement in suspension flows. Soulsby et al. (1994) observed in a tidal current that the vertical sand flux is dominated by the dynamics of the large scale turbulent structures and that the damping of the turbulent kinetic energy is due to the presence of the suspension. Garcia et al. (1995) showed in their open-channel flow study over smooth and transitionally rough beds that ejections are responsible for sediment entrainment into suspension even if the sediments are completely immersed in the viscous sublayer. They concluded that the dynamics of ejections are not affected by the roughness elements confirming a previous result given by Grass (1971). While the last two papers have examined the importance of ejections in lifting up sediments into suspension, the studies of Heathershaw and Thorne (1985), Hogg et al. (1995), Séchet and LeGuennec (1999), investigated the role of sweeps in the event-driven bedload transport of open-channel flows and tidal flows.

The results of these studies confirm the importance of instantaneous shear stresses and their effects near the bed when sediment suspension transport in highly turbulent boundary layers is considered. Classical sediment transport theories based on mean flow quantities (such as the Rouse equation) have been developed at a time when high-resolution instruments were not available. During the last decades, measuring tools able to resolve temporal and spatial scales involved in the turbulent sediment transport mechanism, brought into light new aspects and consequently allow to study the complex turbulent transport phenomenon in more detail. Assessing sediment transport only from mean shear stresses obviously lacks the insight into the underlying physical processes.

The aim of the present study is to provide quantitative information on the effects of coherent structures in the sediment transport mechanism and to validate an expression proposed Cao (1999), of the near bed equilibrium concentration in sediment suspension flows. For this purpose, an extention of the statistical approach used by Nakagawa and Nezu (1977) (hereinafter abbreviated as NN77) for the investigation of the shear stress statistics to mass fluxes is proposed. Quadrant repartitions (obtained from the statistical model and the quadrant threshold technique) of the shear stress will be compared to the quadrant repartition of mass fluxes. Conditional sampling will subsequently be applied to the terms of the advection-diffusion equation in order to quantify the transport capacity of coherent structures. Hence, the contribution to the transport in the sediment concentration profile will be estimated as a function of the threshold level. This is usually considered as the parameter delimiting coherent structures in the flow field.

Finally, the presented instantaneous mass flux profile measurements will permit to evaluate the characteristic scales of the sediment transporting flow structures needed to evaluate directly (no calibration is needed) the near bed equilibrium concentration. Furthermore, a validation method of the used model is reported herein in order to proof its consistency.

2   EXPERIMENTAL DETAILS

The data which will be analyzed here were obtained by in a laboratory study on suspension flow. The experiments were carried out in a recirculating tilting open-channel, 16.8m long, and 0.6m wide (Cellino 1998). The channel bed was rough with a mean roughness of 4.8mm. Special care was taken to ensure steady and uniform flow conditions.

The acoustic sediment flux profiler (APFP; Shen and Lemmin 1997, Hurther and Lemmin 2000a) was employed to measure quasi-instantaneous sediment flux profiles with a sampling frequency of 25Hz and a record length of 180s. The APFP instrument was located 13m from the entrance at the centerline of the channel where turbulence is well developed.

The hydraulic parameters given in Table 1 characterize a highly turbulent subcritical flow of depth $h=12$cm with a bed friction velocity of 3.9cm/s. Quartz-like sediments of $d_{50}=135$ μm and specific density of 2.65 were gradually added to the flow until a layer of sediments, remaining stable during the experiments, appeared on the bed of the channel completely covering the bottom roughness. No more sediments were added from this moment onward because the capacity charge equilibrium condition was reached. In that way the maximum suspension transport capacity of the flow is achieved. Any further supply of sediments will only increase the thickness of the deposition layer on the bed. The reference concentration C_a was measured by a suction device under isokinetical conditions at the water depth $z/h=0.05$.

Table 1 Hydraulic parameters for experiment

Q	h	U	u∗	S	Re$_h$	Fr$_h$	k_g^+	d_{50}	ρ_S	w_0	C_a
(m³/s)	(cm)	(cm/s)	(cm/s)	(×10⁻³)	(×10³)			(mm)	(kg/m³)	(mm/s)	(kg/m³)
0.057	12	0.792	3.9	1	271.2	0.73	6.8	0.135	2650	12	39.33

3   CONDITIONAL STATISTICS

We define the following variables: u', w', c' are the zero mean fluctuating longitudinal, and vertical velocity and concentration components, respectively. $\hat{u}, \hat{w}, \hat{c}$, are equal to $u'/\sqrt{\overline{u'^2}}, w'/\sqrt{\overline{w'^2}}, c'/\sqrt{\overline{c'^2}}$. We shall quantify the contributions of the relative shear stress for the covariance term $\varepsilon_1 = u'w'/\overline{u'w'}$ and the contribution of the relative mass fluxes for $\varepsilon_2 = c'u'/\overline{c'u'}$ and $\varepsilon_3 = c'w'/\overline{c'w'}$. Fig.1 shows the orientation of the quadrants in the respective planes. Three joint probability density functions $p_1 = (\hat{u}, \hat{w}), p_2 = (\hat{c}, \hat{u})$, and $p_3 = (\hat{c}, \hat{w})$ given as the inverse Fourier transforms of the characteristic functions $\phi_1 = (\hat{u}, \hat{w}), \phi_2 = (\hat{c}, \hat{u})$, and $\phi_3 = (\hat{c}, \hat{w})$ respectively, can be expressed as functions of the moment and cumulant generating functions in which $m_{1,jk} = \overline{\hat{u}^j \hat{w}^k}, m_{2,jk} = \overline{\hat{c}^j \hat{u}^k}$, and $m_{3,jk} = \overline{\hat{c}^j \hat{w}^k}$ denote the moments of $(j+k)^{th}$ order and $k_{1,jk}, k_{2,jk}$ and $k_{3,jk}$ correspond to the cumulants of $(j+k)^{th}$ order. By limiting these cumulant expansion series to an order of three, NN77 determined the conditionally sampled probability densities of covariance events ε_1 over the four quadrants from a high order cumulant discard Gram-Charlier probability density function. The mathematical manipulation is described in detail in NN77. The following general equations are given:

$$p_{i,2}(\varepsilon_i) = p_{i,N}(\varepsilon_i) + \varphi_i^-(\varepsilon_i) \quad p_{i,4}(\varepsilon_i) = p_{i,N}(\varepsilon_i) - \varphi_i^-(\varepsilon_i) \quad (\varepsilon_i > 0) \quad i = 1,2$$

$$p_{i,1}(\varepsilon_i) = p_{i,N}(\varepsilon_i) + \varphi_i^+(\varepsilon_i) \quad p_{i,3}(\varepsilon_i) = p_{i,N}(\varepsilon_i) - \varphi_i^+(\varepsilon_i) \quad (\varepsilon_i < 0) \quad (1)$$

where the index q in $p_{i,q}$ denotes the quadrant index (1 to 4) in the ith plane with planes 1, 2 and 3 corresponding to the (u', w') and (c', u') planes, respectively. The probability density $P_{i,N}(\varepsilon_i)$ is directly developed from the corresponding bivariate normal distribution (Hurther and Lemmin 2000b). From Eq.(1) we will calculate the first order moment $R_{i,q}$ and the time fraction $T_{i,q}$ of each conditional probability density distribution as a function of the threshold level H_i. By increasing the level of H_i, progressively stronger fractional ε_i events will be selected. The parameters $R_{i,q}$, and $T_{i,q}$, evaluated from the probability densities will be compared to those from experimental results in order to obtain information on the quadrant distribution of the relative covariances. Consequently, the relative contribution $R_{i,5}$ and time fraction $T_{i,5}$ of the events having relative shear ε_i lower than the defined thresholds are called the hole event.

4   QUADRANT CONTRIBUTION OF SHEAR STRESS AND MASS

FLUXES

Figs.2-4 show the relative magnitude of shear stress, horizontal and vertical mass fluxes, respectively, as functions of the corresponding selection criteria H_i. The theoretical (from Eq.(1)) and experimental results are given for three different flow depths in the wall, intermediate and free surface flow regions. The time fraction of the hole events at those three depths are also presented in each figure.

The quadrant dynamics of the three investigated quantities is obviously dominated by the contribution of two quadrants. In Fig.2, ejections (quadrant two) and sweeps (quadrant four) dominate, in accordance with results given in the literature. For example, the experimental contributions of quadrants two and four in Fig.2 at *z/h*=0.85 for H_1=0 are equal to 1.1 and 0.76, respectively, which are in agreement with the values of 1 and 0.65 at *z/h*=0.772 given by NN77.

Another well documented characteristic of the bursting phenomena is the distribution of the hole event time fraction of the relative contribution. For example in Fig.2 at *z/h*=0.32 and H_1=5, the hole event time fraction is equal to 85%, meaning that only 15% of the events still contribute to 40% of the shear stress in quadrant two and 35% of the shear in quadrant four revealing the short lifetime and large amplitudes of the turbulence producing events. These observations are in agreement with several experimental studies (Nakagawa and Nezu 1981; Luchik and Tiederman 1987) concerning the bursting process in clear water turbulent boundary layers. Here we have demonstrated that these characteristics of shear stress dynamics in suspension flow under capacity charge condition are very similar to those in clear water flow.

From the observed probability density functions, the important contributors to the horizontal mass fluxes are identified as quadrant two and four events (Fig.3). The quadrant four contribution is more important than the quadrant two contribution for any H_2 which indicates that ejections entrain more sediments than sweep events. An association of quadrant four horizontal mass flux structures with ejections can be suggested. When an ejection occurs (i.e. with *u'*<0), it will lift up sediments from a region of higher mean concentration to one of lower mean concentration. The same reasoning holds for the combination of quadrant two horizontal mass fluxes with sweeps.

The quadrant contributions of the vertical mass fluxes are presented in Fig.4. Here, quadrant three and one events are associated with ejections and sweeps, respectively. The experimental curves are fairly well described by the theoretical third order model. The order of magnitude of the relative contributions of vertical and horizontal mass fluxes versus H_2 and H_3 correspond to the relative shear stress contributions.

Therefore, the general quadrant dynamics, including the hole event time fraction, of the mass fluxes and shear stress are in good agreement. This indicates the importance of the bursting process in the sediment transport dynamics.

5   TRANSPORT CAPACITY OF COHERENT STRUCTURES

In this section, we will evaluate the contribution of coherent structures to the concentration profile by considering the conditionally sampled diffusion equation for the sediments which can be expressed in its general formulation as:

$$\frac{\partial \langle c \rangle_H}{\partial z} = \frac{1}{w_0} \left[\frac{\partial \langle cu \rangle_H}{\partial x} + \frac{\partial \langle cv \rangle_H}{\partial y} + \frac{\partial \langle cw \rangle_H}{\partial z} \right] \qquad (2)$$

where $\langle \rangle_H$ denotes an averaging over the structures delimited by the selection criteria H_1. w_0 represents the mean settling velocity of the sediments in pure, still, clear water. The Reynolds decomposition of the variables is not applied to avoid the ambiguous definition of the mean velocity when conditional sampling is undertaken.

The different terms of Eq. (2) for different values of H_1 are given in Fig.5. For $H_1=0$, no particular flow structures are selected and the longitudinal gradient of the mean horizontal mass flux is obviously negligible compared to the vertical gradient of the mean vertical mass flux. The equilibrium between the mean ascending sediment mass flux caused by the entrainment capacity of coherent structures and the deposition flux due to the effect of gravity is evident.

Fig.6 shows the concentration profiles relative to the reference concentration (taken at z/h=0.05) for several threshold levels H_1 and the quadrant repartition diagrams of the relative vertical mass flux sampled as a function of H_1 and H_3 at z/h=0.16, z/h=0.5, z/h=0.83. From this figure, the dynamics of the relation of the instantaneous vertical mass flux to the instantaneous shear stress events can be investigated in more detail.

Along the whole water column, the transport capacity of the coherent structures decreases proportionally with increasing *H*. For values of $H_1 = 3$ and $H_1 = 5$, which represent strong structures, the transport capacity of coherent structures is still equal to 49% and 31% of the total transport, respectively. Combining this information with the hole events time fraction given in the quadrant repartition diagrams, the time fraction of these coherent structures for the same two H_1 values are found to be only 30% and 10%, respectively. From this example, the importance of coherent structures in the sediment suspension mechanism becomes quantitatively evident, even if their lifetime is relatively short.

In quadrant one, corresponding to ejection events, good agreement is found between the vertical mass fluxes sampled as functions of H_1 and H_3 for all three depths. This indicates that the upward mass flux is directly correlated with ejection events for all values of H_1 and H_3 throughout the whole water column. Sediment resuspension from the bed is strongly controlled by ejections even though their time fraction quickly becomes relatively small with increasing *H*. In quadrant three which corresponds to sweeps, good agreement is again found for the functions of H_1 and H_3. However, at all depths but more so when approaching the channel bed, the fall-off with increasing *H* is

more rapid than for the ejection events. Sweeps are obviously predominantly organized in low H events.

Ejections and sweeps also influence the sediment flux in quadrants two and four, evident from the contributions below the solid lines in those quadrants. The contribution of interaction events of quadrants two and four is represented by the difference between the solid line and the dotted line in Fig. 6. It is obvious that interactions are hardly correlated with the vertical mass fluxes. Therefore, interaction events can be ignored in the sediment transport and do not contribute to transport capacity curves of Fig. 6

6   NEAR BED EQUILIBRIUM CONCENTRATION FORMULATION
BASED ON SCALES OF COHERENT STRUCTURES

Cao (1999) has proposed an expression for the equilibrium near bed concentration C_a based on scales of turbulent bursts. This is a significant improvement over existing empirical formulations (VanRijn, 1984 , Zyserman and Fredsoe, 1994). He gives a relation for the bed sediment entrainment function E in which the outer-scale law is used for the determination of the normalized turbulent bursting period. However, as pointed out by Cao (1999), a direct validation of the proposed near bed sediment entrainment function was not possible because quantitative data for sediment entrainment under different particle size and hydraulic conditions is lacking. Instead, the author has undertaken a calibration based on existing literature data, to determine the bursting parameter T_E^+/A_C , in the following formulation:

$$C_a = \frac{A_C}{T_E^+} \frac{C_0 d_{50}}{\omega_0 \theta_c} \frac{(\theta - \theta_c)U_\infty}{h} \qquad (3)$$

C_a, A_C, C_0, d_{50}, θ, θ_c, T_E^+ , w_0, h are the equilibrium near-bed volumetric concentration of particles, the mean bed surface fraction per unit area of all bursts, particle volumetric concentration of the bed, the diameter of the particles, the Shields parameter due to skin friction, the critical Shields parameter for initial motion of particle, the outer-scale-based dimensionless bursting period, the settling velocity of a single particle in still water, the water depth, respectively.Based on our ability to evaluate the bursting characteristics directly from the measurements, we will verify and discuss Eq.(3).

T_E^+ is estimated by conditionally sampling the instantaneous velocity field with a half-value shear stress threshold as defined by Nezu and Nakagawa (1993) (we will refer this sampling condition as "NN50" hereinafter). Hence, in Eq.(3), it is implied that the total deposition flux at the equilibrium near bed level is caused by the conditionally sampled entrainment due to bursts which are stronger than NN50. A priori, that hypothesis is not obvious since there is no physical reason that weaker bursts should not contribute to the deposit. In order to investigate this point we start by calculating the dependence of different relative parameters on the threshold parameter H_1 at depth z/h=0.08 which is close to the equilibrium depth (z/h=0.05). The paramenters R_1, R_2 and T_5 represent the mean shear stress contribution, the mean vertical mass flux, and the time fraction of the unselected flow part, respectively (the quadrant index q disappeared since here, the parameters are integrated over all the quadrants). Concerning the mean contributions of

shear stress and vertical mass flux, the relative vertical mass flux R_2 is found to be lower than the relative shear stress contribution R_1 (Fig.7). As discussed in section 5, this difference originates from the de-correlation between downward mass fluxes and sweeps moving towards the wall while ejection events are always highly correlated with ascendant mass flux events over the entire flow depth. As a consequence, the outer-scale formulation of the volumetric near bed concentration for low sediment concentration (Eq. (3)) should be corrected with a factor of 0.6 on the right hand side. Finally, the validation of the proposed corrections can be achieved by comparing the surface portion of the bursts per unit bed area, A_C, estimated with Eq. (3) and the corrected one. These results can be compared to the well-accepted measurements of Kline et al. (1967) and Kim et al. (1971) which yield a value of $A_C = 0.02$. The Following results have been obtained for the parameter A_C: 0.043 and 0.026 with the use of Eq. (3) and the corrected one, respectively. Obviously, better agreement with the value of 0.02 is found using the corrected formulation.

7   SUMMARY AND CONCLUSIONS

A third order cumulant discard Gram-Charlier probability density function has been applied to the shear stress, as well as the horizontal and vertical turbulent mass fluxes in order to quantify their quadrant dynamics. Good agreement was found between the model results and the experimental estimations in the wall and intermediate flow regions.

The shear stress quadrant dynamics correspond to results found in the literature with a clear dominance of quadrant two (ejections) and quadrant four (sweeps) events. Thus, the presence of sediments in the flow, even at capacity charge, does not influence the flow dynamics on the scales of coherent structures. Instead, a quadrant repartition similar to the shear stress distribution is observed for the mass fluxes and the effect of the hole size parameter H on the mass fluxes is comparable to that of the shear stress. This shows that the mass fluxes are also strongly organized in coherent structures. The quadrant repartition obtained for the mass fluxes can be interpretated through the suspended sediment entrainment capacity of ejections and sweeps.

Based on the conditionally sampled sediment diffusion equation, the suspended sediment transport capacity of coherent structures has been quantified. The proportion of the relative sediment concentration profile (relative to the near bed reference concentration taken at z/h=0.05) and the time fraction were estimated as functions of the shear stress threshold level (delimiting the coherent structures in the instantaneous flow field). It has been shown quantitatively that coherent structures are important contributors to suspended sediment transport. Strong structures which are only present for 30% of the time carry nearly 50% of the vertical sediment flux. This indicates that sediment transport is highly intermittent and that sediment concentration in the water column varies strongly.

Based on these results, a novel bursting scales dependent formulation of the near bed equilibrium concentration given by Cao (1999) has been corrected.

Further investigations are needed to determine whether the suspended sediment transport capacity of coherent flow structures in highly turbulent boundary layers is

universal. In other words, is a general characterization of the flow structures transporting suspended sediments possible? Cao (1999) has demonstrated that such a concept can be applied for the near bed equilibrium concentration prediction in suspension flows. An extension of this approach to the concentration profile prediction would lead to a completely new model for the sediment transport assessment in suspension flows based on coherent structure characteristics.

Acknowledgements

References

Cao Z (1999) Equilibrium near-bed concentration of suspended sediment. J Hydr. Engrg. 125: 1270-1278.

Cellino M (1998) Experimental study of suspension flow in open channels. PhD thesis. Ecole Polytechnique Fédérale de Lausanne.

Garcia M; Niño Y; López F (1995). Coherent flow structures in open channels, Leeds, U.K., (J Wiley & Sons Ltd.)

Grass AJ (1971) Structural features of turbulent flow over smooth and rough boundaries. J of Fluid Mech. 50: 233-255.

Heathershaw AD; Thorne PD (1985) Sea bed noises reveal role of turbulent bursting phenomenon in sediment transport by tidal current. Nature 316: 339-342.

Hogg AJ; Dade WB; Huppert HE; Soulsby RL (1995). Coherent flow structures in open channels, Leeds, U.K., (J Wiley & Sons Ltd).

Hurther D; Lemmin U (2000a) A correction method of turbulence measurements with a 3D-ADVP. Journal of Atmospheric and Oceanic Technologies (in press).

Hurther D; Lemmin U (2000b) Shear stress statistics and wall similarity analysis in turbulent boundary layers using a high resolution 3-D ADVP. IEEE Journal of Oceanic Engineering (in press).

Kim, H. T., S. J. Kline, et al. (1971). "The production of turbulence near a smooth wall in a turbulent boundary layer." J. Fluid Mech. 50(133-160).

Kline, S. J., W. C. Reynolds, et al. (1967). "The structure of turbulent boundary layers." J. Fluid Mech. 30(4): 741-773.

Lu SS; Willmarth WW (1973) Measurements of the structure of the Reynolds stess in a turbulent boundary layer. J Fluid Mech. 60: 481-511.

Luchik TS; Tiederman WG (1987) Timescale and structure of ejection and bursts in turbulent channel flows. J Fluid Mech. 174: 529-552.

Nakagawa H; Nezu I (1977) Prediction of the contribution to the Reynolds stress from bursting events in open-channel flows. J Fluid Mech. 80: 99-128.

Nakagawa H; Nezu I (1981) Structure of space-time correlations of bursting phenomena in an open-channel flow. J Fluid Mech. 104: 1-43.

Raupach MR (1981) Conditional statistics of Reynolds stress in rough wall and smooth wall turbulent boundary layers. J Fluid Mech. 108: 363-382.

Séchet P; LeGuennec B (1999) Near wall turbulent structures and bedload transport. J of Hydr. Res.

Shen C; Lemmin U (1997) A two-dimensional acoustic sediment flux profiler. Meas. Sci. Technol. 8: 880-884.

Soulsby RL; Atkins R; Salkield AP (1994) Observations of the turbulent structures of a suspension of sand in a tidal current. Continental Shelf research 14: 429-435.

Van Rijn, L. C. (1984). "Sediment transport, part II: Suspended load transport." J. Hydr. Engrg., 110(11): 1613-1641.

Zyserman, J. A. and J. Fredsoe (1994). "Data analysis of bed concentration of suspended sediment." J. Hydr. Engrg., 120(9): 1021-1042.
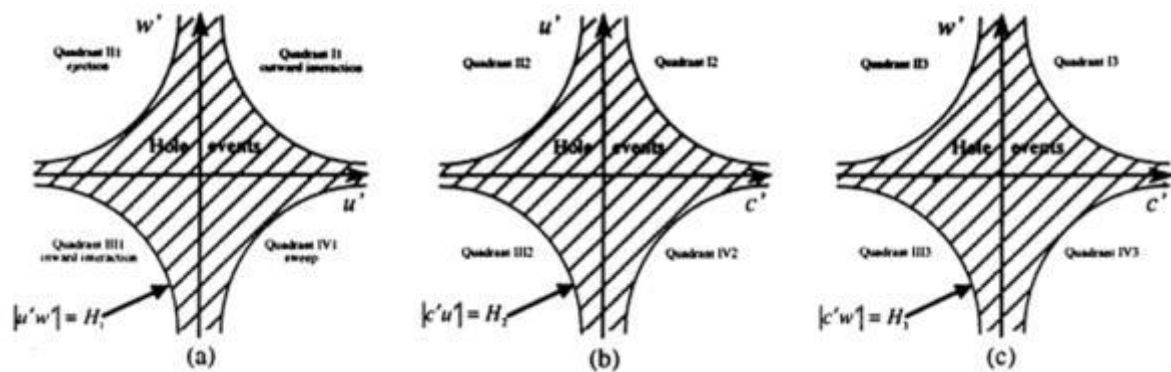
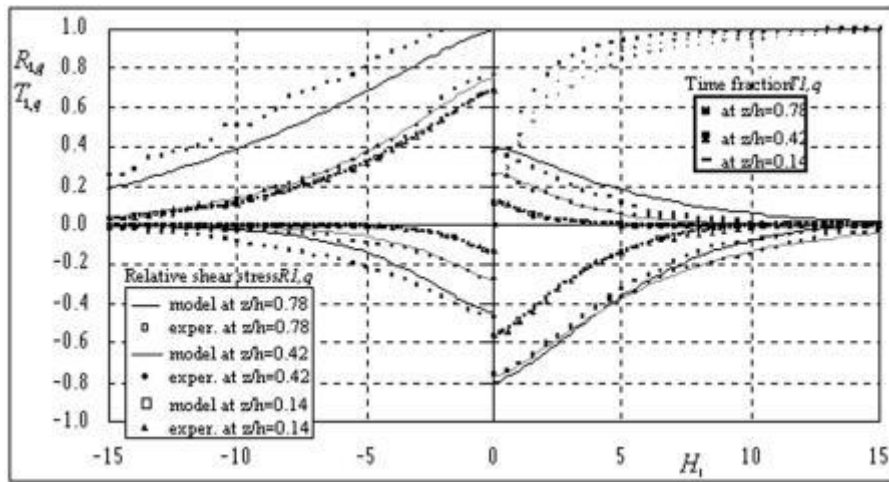Fig.1   Division of events. (a) shear stress, (b) horizontal mass flux and (c) verical mass flux

Fig.2 Theoretical and experimental quadrant repartition of relative shear stress ε_1 in function of threshold criteria H_1
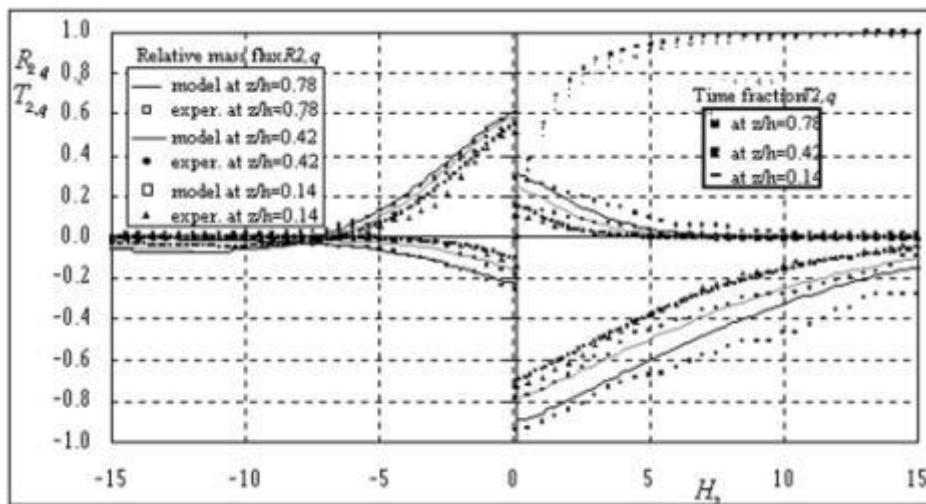

Fig.3 Theoretical and experimental quadrant repartition of relative shear stress ε_2 in function of threshold criteria H_2
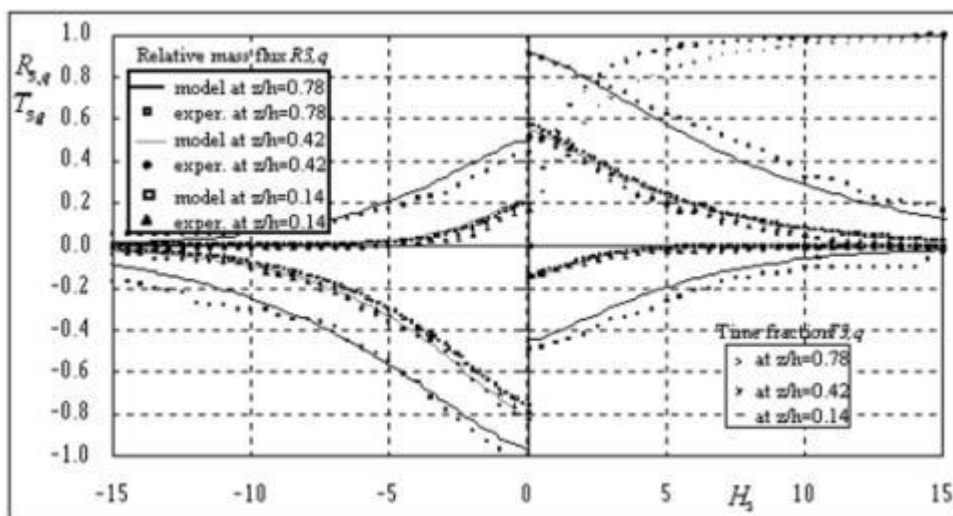
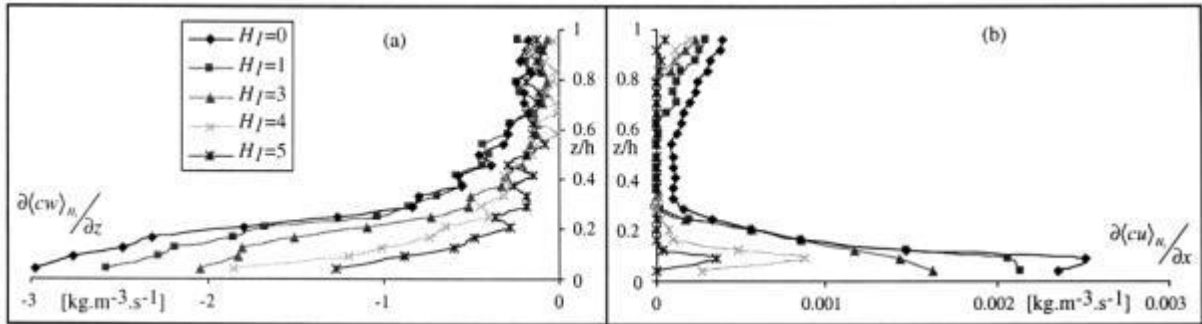Fig.4 Theoretical and experimental quadrant repartition of relative shear stress ε_3 in function of threshold criteria H_3

Fig.5 Conditional sampled terms of the sediment diffusion equation. (a) vertical mass flux gradient (b) horizontal mass flux gradient
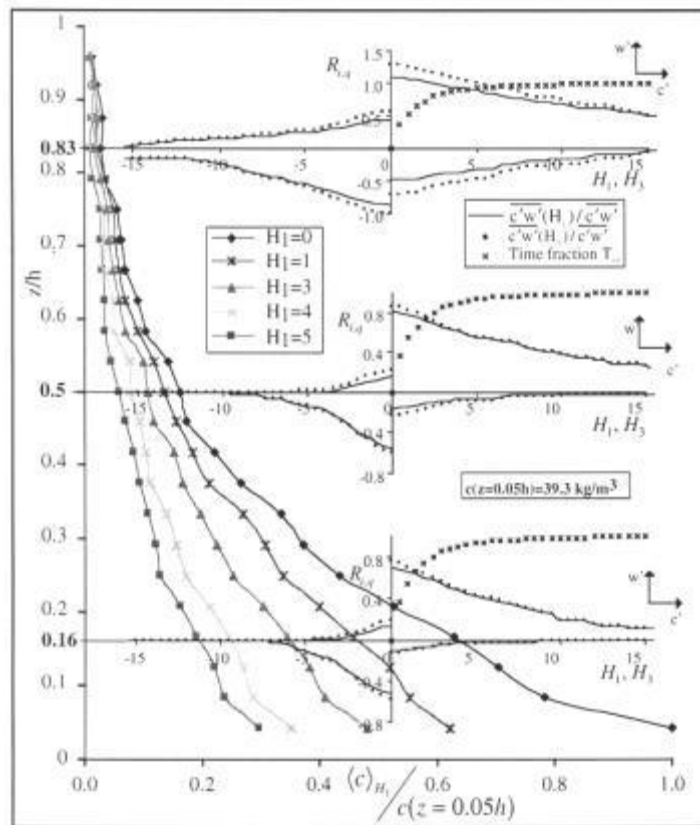

Fig.6 Transport capacity in function of threshold level H_1 and quadrant distribution of c'w' in function of H_3 (dotted lines) and H_1 (solid lines) at three different depths.
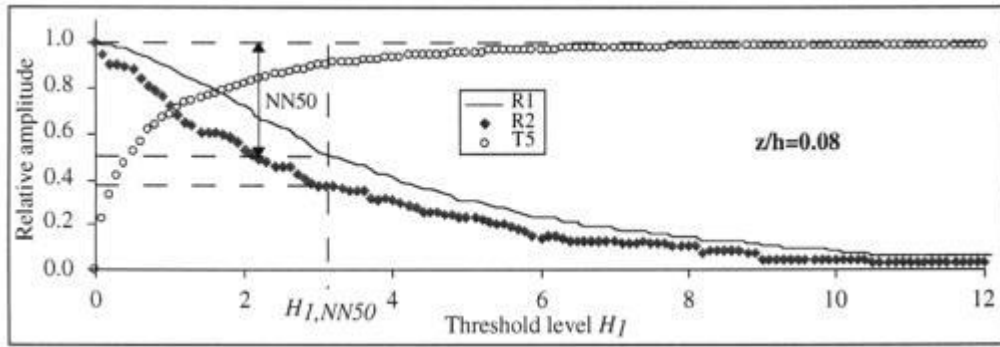
Fig.7 Relative shear stress R_1, relative vertical mass flux R_2 and time fraction T_5 of unselected events versus threshold value H_1.